

# FlexAM: Flexible Appearance-Motion Decomposition for Versatile Video Generation Control

Mingzhi Sheng<sup>1\*</sup> Zekai Gu<sup>2\*</sup> Peng Li<sup>2</sup> Cheng Lin<sup>3</sup> Hao-Xiang Guo<sup>4</sup>  
 Ying-Cong Chen<sup>1,2†</sup> Yuan Liu<sup>2†</sup>

<sup>1</sup>HKUST(GZ) <sup>2</sup>HKUST <sup>3</sup>MUST <sup>4</sup>Tsinghua University

<https://github.com/IGL-HKUST/FlexAM>

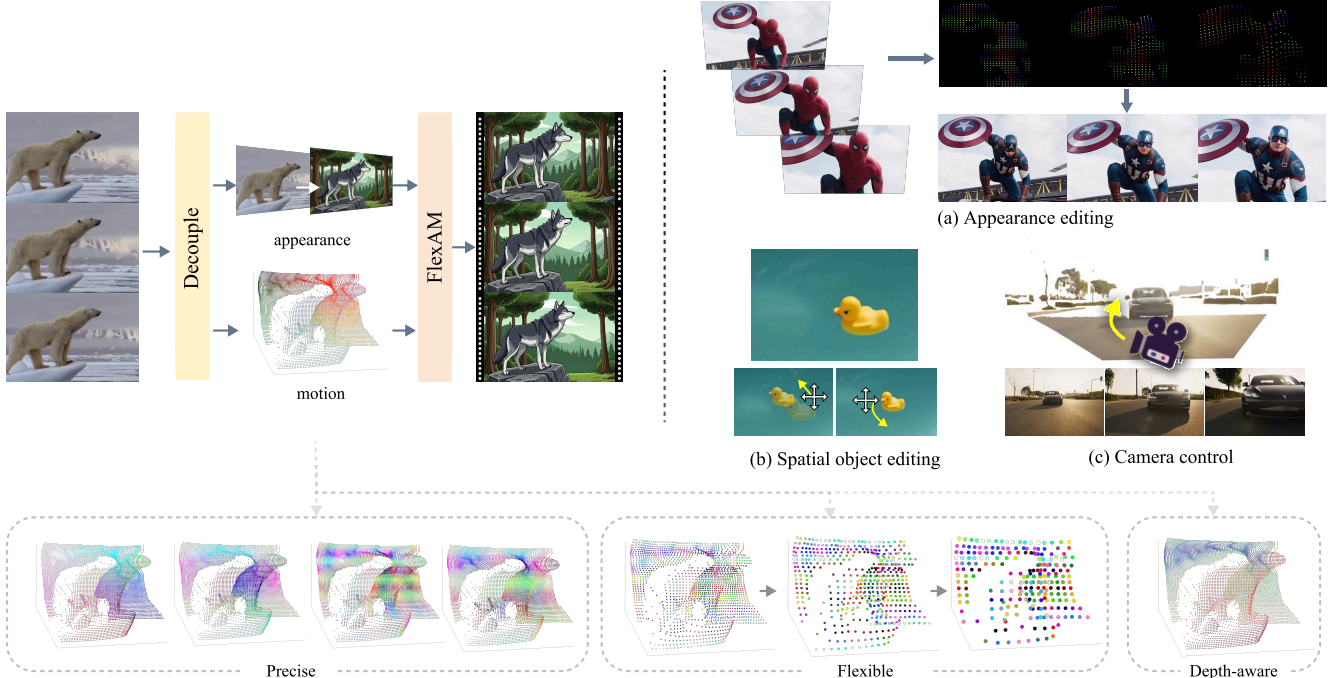


Figure 1. **FlexAM** treats controllable video generation as a fundamental disentanglement of appearance and motion. It defines a novel 3D control signal, based on a dynamic point cloud, that explicitly represents motion with flexible, precise, and depth-aware. This approach allows FlexAM as a unified model to achieve a wide range of tasks, including I2V/V2V editing, camera control, and spatial object editing.

## Abstract

*Effective and generalizable control in video generation remains a significant challenge. While many methods rely on ambiguous or task-specific signals, we argue that a fundamental disentanglement of “appearance” and “motion” provides a more robust and scalable pathway. We propose FlexAM, a unified framework built upon a novel 3D control signal. This signal represents video dynamics as*

*a point cloud, introducing three key enhancements: multi-frequency positional encoding to distinguish fine-grained motion, depth-aware positional encoding, and a flexible control signal for balancing precision and generative. This representation allows FlexAM to effectively disentangle appearance and motion, enabling a wide range of tasks including I2V/V2V editing, camera control, and spatial object editing. Extensive experiments demonstrate that FlexAM achieves superior performance across all evaluated tasks. Codes and more results are available at [FlexAM](https://github.com/IGL-HKUST/FlexAM).*

\*Equal contribution.

†Corresponding authors.

## 1. Introduction

The field of video generation has witnessed remarkable breakthroughs in recent years. Beyond the typical text-to-video [11, 18, 37] and image-to-video [11, 28, 29] paradigms, controllable video generation [4, 7, 15, 17, 19, 21, 22, 24] has emerged as a significant area of research, spawning a multitude of downstream tasks. These include, for instance, reference-image-based [4, 6, 14, 20] and reference-audio-based [8, 30, 36] video synthesis. This rapid evolution underscores the dynamic and intricate nature of the field.

To enhance controllability, researchers have explored decomposing videos into various elemental signals. Prior works have often focused on specific tasks by isolating particular signals, such as skeletons [5, 36], optical flow [24], depth [7, 17], camera motion [2, 3, 12, 31, 33], and object trajectories [9, 10, 35, 38]. While some studies have attempted to combine these disparate modalities for compositional control [5, 15, 16, 21, 22], we argue that such approaches are often inefficient. They typically require bespoke training data and model designs for each new control signal, which complicates the pipeline and limits scalability. This presents a challenge in finding a unified control signal that is both comprehensive and efficient.

A more fundamental approach is to decompose video into “appearance” and “motion”. We posit that this disentanglement is essential for robust controllable generation, as “motion” is a generalizable concept that can encapsulate human pose, camera movement, and object dynamics. Furthermore, this separation allows for the use of independent tools to edit either appearance or motion. A recent work, Diffusion as Shader (DaS) [10], adopted this philosophy, interpreting a video as the appearance of its first frame combined with the subsequent motion of a 3D point cloud. This allowed for versatile control by manipulating the motion signal.

However, existing appearance-motion decomposition methods suffer from significant limitations. A truly effective decomposition must satisfy several criteria. First, its appearance conditioning should be able to describe and maintain the appearance of any region across time, not just the first frame. The approach in DaS [10], for example, struggles to model objects that appear later in the sequence. Second, its motion signal must be: (1) **flexible**, supporting both dense and sparse representations; (2) **precise**, capable of distinguishing the similar motions of closely adjacent 3D points; and (3) **depth-aware**, explicitly encoding changes in object proximity relative to the camera.

To address these challenges, we propose FlexAM, a unified framework built upon a novel appearance-motion decomposition. For appearance, FlexAM moves beyond first-frame conditioning by accepting arbitrarily masked video (or individual frames) as the appearance condition. This

allows it to seamlessly execute tasks including image-to-video synthesis, masked video-to-video editing, and arbitrary combinations thereof. For motion, we construct a superior motion control signal based on the 3D tracking video from DaS [10], termed an enhanced “motion video”, composed of a set of motion trajectories, which uses the XYZ coordinates of these points in the first frame to define the trajectory colors. (1) To achieve high precision and distinguish adjacent elements, the pixel color is determined by the point’s 3D coordinates in the first frame’s camera system, encoded using multi-frequency positional encoding across multiple layers. (2) To ensure the signal is depth-aware, we introduce additional explicit layers that represent the depth variations of these points over time, enabling the model to better reason about 3D structure and occlusion. (3) FlexAM supports varying point densities to represent motion, enabling it to flexibly balance precision and generalization to meet diverse task requirements. This is achieved through a training strategy that involves varying degrees of downsampling on the 3D control signal. In summary, our contributions are as follows:

1. We propose a comprehensive and general-purpose 3D control signal. By abstracting video motion into a colored dynamic point cloud and using precise multi-frequency positional encodings to distinguish adjacent elements, it explicitly represents the 3D spatio-temporal motion of elements. This enables our model to precisely control the motion and trajectories of elements during generation and editing, facilitating tasks such as camera control and object manipulation.
2. Our method effectively disentangles video appearance and motion. This mechanism allows for the independent editing of appearance and motion for any part of an input video or image.
3. We employ a training strategy that involves varying degrees of downsampling on the 3D control signal. This allows the model to learn to balance precision and generalization, keeping flexible and adapting to the demands of different tasks.

We conduct extensive experiments comparing FlexAM with baseline methods on tasks including controllable video generation and editing, camera control, and spatial object editing. The results demonstrate that FlexAM surpasses all baselines and achieves state-of-the-art (SOTA) performance across all evaluated tasks.

## 2. Related Work

### 2.1. Controllable Video Generation

Recent advancements in video diffusion models have achieved high-fidelity, temporally coherent video generation [18, 29, 37], spurring research into controllable video synthesis. Early efforts focused on specific modalities [3, 7,

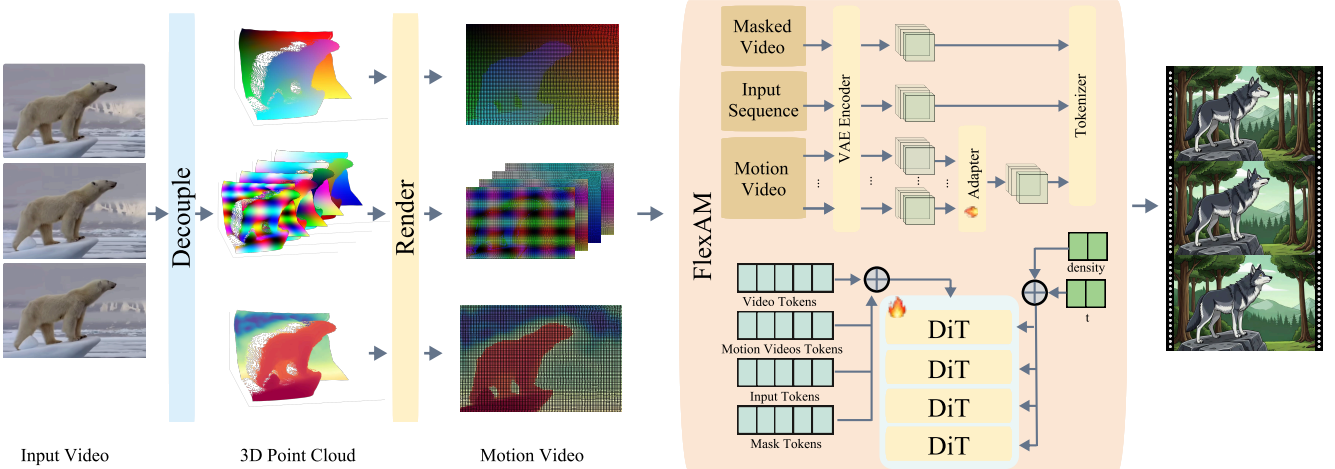


Figure 2. The FlexAM pipeline. Our approach disentangles video generation into appearance and motion control. The input video is first processed to create a 3D point cloud, which is then rendered into a motion video with multi-attributes, serving as the motion control signal. This motion control signal, along with a masked input video (for appearance control), is fed into the FlexAM generative model. FlexAM processes these control signals—via VAE encoders, Adapter, and a tokenizer—alongside video, motion, input, and mask tokens. The model then generates a new video by integrating these decoupled appearance and motion controls, as illustrated by the example of transforming a polar bear video into a wolf video while maintaining motion dynamics.

21, 24, 33, 38], such as using poses or skeletons for human-centric animation [4, 5, 23], or audio for talking heads and sound-synchronized scenes [8, 30, 36]. More recent paradigms include trajectory-based control, where users specify 2D motion paths [9, 35, 38], and 3D-aware control, targeting cinematic camera or unified human-camera motion [2, 3, 12, 31, 33]. Despite this progress, most existing methods are designed for a single type of control and often rely on 2D signals, which can be ambiguous when representing complex 3D spatial dynamics.

## 2.2. Appearance Editing

Appearance editing aims to modify visual attributes, such as object identity or style, while preserving the original motion. A key challenge in this task is effectively decoupling the appearance and motion. Previous approaches use various strategies to achieve this. Video-P2P [21] and follow-your-motion [22] adapt an image model using cross-attention control. MagicEdit [17], Motion Prompting [9], and MotionCtrl [33] explicitly disentangle content, structure, and motion during training. However, these methods often rely on intermediate 2D representations. These 2D signals are usually lossy and lack 3D spatial context, leading to ambiguities and artifacts during complex motion. More comprehensive frameworks like VACE [15] aim for versatility but are not truly unified, requiring users to prepare a cumbersome and diverse set of conditions, such as depth maps, skeletons, or masks. FlexAM addresses these limitations by using the motion video as an explicit representation of the underlying dynamics. This single, 3D-

aware signal avoids both the ambiguity of 2D representations and the complexity of multiple conditions. By conditioning on this unified signal, our model preserves the exact 3D motion while robustly propagating the new appearance to the masked regions.

## 2.3. Camera Control

Precise camera control is essential for cinematic storytelling and requires a strong understanding of 3D scene geometry. Recent works, however, often specialize in distinct sub-tasks. For instance, CineMaster [31] and CameraCtrl [12] present 3D-aware frameworks for I2V/T2V generation with controllable trajectories, while ReCamMaster [2] focuses on V2V re-rendering. This specialization means I2V-focused models cannot perform V2V re-cinematography, and vice versa. Other methods have explored different avenues for 3D-aware control. DaS [10] aimed for versatile control, including camera manipulation, using a 3D tracking video. However, these methods suffer from limitations, including early 3D-aware models, which implicitly infer 3D structure, leading to potential depth ambiguity. The 3D tracking signal lacked explicit, time-varying depth information, which resulted in instabilities during precise camera control. This highlights the need for a framework that not only unifies I2V and V2V camera control but also relies on a 3D signal that is robust against geometric ambiguity.

## 2.4. Spatial Object Editing

Spatial object editing involves manipulating the 3D position, rotation, and trajectory of specific objects within a

scene. Some 3D-aware methods approach this task by focusing on explicit geometry. GeoDiffuser [27] enables object manipulation by directly editing the scene’s depth maps. While this provides explicit 3D control, such an approach can lack flexibility. DaS [10] introduced 3D tracking videos as a promising 3D-aware control signal. However, this earlier 3D representation lacked sufficient depth detail to resolve complex 3D relationships, leading to spatial inconsistencies. FlexAM addresses this limitation by proposing a more comprehensive and flexible 3D control signal, encoding richer spatial and depth information to achieve fine-grained, spatially-consistent object manipulation.

### 3. Method

Our approach, FlexAM, is built upon the key insight of disentangling video into two fundamental components: appearance and motion. This separation is pivotal, as it permits the independent editing of either part. FlexAM can then utilize these edited representations as control signals to the generative model, enabling targeted adjustments to the video’s appearance or motion while keeping another part of the video consistent. We first detail our representations for appearance (Sec. 3.1) and our novel motion video (Sec. 3.2), followed by the architecture that integrates them (Sec. 3.3).

#### 3.1. Appearance Control Signal Representation

We define the appearance broadly to accommodate diverse generations and editing tasks. Unlike methods conditioned solely on a single first frame, FlexAM accepts a partially masked video  $\mathbf{V}_{\text{masked}} \in \mathbb{R}^{T \times H \times W \times 3}$  as the appearance condition. In this formulation, known or unedited regions retain their original pixel values, while regions or frames targeted for generation or editing are filled with gray value 127. This flexible representation allows the model to naturally handle tasks ranging from image-to-video, where all frames except the first are masked, to video-to-video editing, where only specific spatio-temporal regions are masked, all within a unified framework.

#### 3.2. Motion Control Signal Representation

Similar to DaS [10], we represent video motion using a dynamic point cloud. These points, extracted from the source video’s dynamics, are endowed with multi-dimensional attributes designed for precise, depth-aware, and flexible control. As shown in the left part of Figure 2, this attributed point cloud is then rendered into a video representation  $\mathbf{C} \in \mathbb{R}^{T \times H \times W \times 3}$ , which we term the motion video, to serve as our motion control signal.

Specifically, the motion video describes the dynamics of a set of 3D points  $\{\mathbf{p}_i(t) \in \mathbb{R}^3\}$ , where  $t$  is the frame index. Each point  $\mathbf{p}_i(t) = (x_i(t), y_i(t), z_i(t))$  corresponds to a specific spatial region. To create the final control signal, these points are projected onto the 2D screen space.

At each projected location  $(u_i(t), v_i(t))$ , we populate attribute vector  $\mathbf{A}_i(t)$ . All unprojected locations are set to zero. This attribute vector  $\mathbf{A}_i(t)$  is composed of four components, strategically designed to be precise, depth-aware, and flexible.

**Precise Positional Encoding** To precisely distinguish adjacent points and capture fine-grained spatial relationships, we encode the initial 3D coordinates. This includes an identity positional encoding  $\mathbf{f}_{\text{identity}} \in \mathbb{R}^3$ , which stores the normalized initial coordinates  $(x'_i(0), y'_i(0), z'_i(0))$ , where  $z'$  represents inverse depth. Additionally, we compute a multi-frequency positional encoding  $\mathbf{f}_{\text{freq}} \in \mathbb{R}^{12}$ . This is formed by applying a 4-level cosine function  $\gamma(v) = (\cos(2^l \pi v))_{l \in \{0,1,2,3\}}$  to each of the three initial coordinates.

**Depth-aware Representation** To explicitly encode 3D structure and resolve depth ambiguity, we include a depth-aware encoding  $\mathbf{f}_{\text{depth}} \in \mathbb{R}^3$ . This component represents the current normalized depth  $z''_i(t)$  at time  $t$ , which is mapped to an RGB vector using the Spectral colormap  $\mathcal{S}(\cdot)$ .

**Control Flexibility and Masked Editing** A binary edit mask  $\mathbf{f}_{\text{mask}} \in \mathbb{R}^1$ , represented by  $m_i(t)$ , is included to indicate specific regions targeted for editing. The full attribute vector  $\mathbf{A}_i(t)$  at the projected location  $(u_i(t), v_i(t))$  is the concatenation of these components:

$$\mathbf{A}_i(t) = \left( \mathbf{f}_{\text{identity}}^{(i)}, \mathbf{f}_{\text{freq}}^{(i)}, \mathbf{f}_{\text{depth}}^{(i,t)}, \mathbf{f}_{\text{mask}}^{(i,t)} \right) \in \mathbb{R}^{19}, \quad (1)$$

where

$$\mathbf{f}_{\text{identity}}^{(i)} = (x'_i(0), y'_i(0), z'_i(0)) \quad (2)$$

$$\mathbf{f}_{\text{freq}}^{(i)} = (\gamma(x'_i(0)), \gamma(y'_i(0)), \gamma(z'_i(0))) \quad (3)$$

$$\mathbf{f}_{\text{depth}}^{(i,t)} = \mathcal{S}(z''_i(t)) \quad (4)$$

$$\mathbf{f}_{\text{mask}}^{(i,t)} = m_i(t). \quad (5)$$

Thus, the motion video is a 19-channel video representation synthesized by aggregating these attributes. It comprises 18 channels derived from the identity, 4-level frequency, and depth-aware encodings (organized as 1 + 4 + 1 three-channel rendered streams), along with a 1-channel binary mask  $\mathbf{f}_{\text{mask}}$ .

A key feature of the motion video is its flexibility. The signal can represent motion densely or sparsely, determined by the number of points  $\{\mathbf{p}_i(t)\}$  used. This allows FlexAM to balance precision and generalization. As detailed in Sec. 3.3, we train the model to handle this variability by stochastically down-sampling the point clouds during training.

#### 3.3. Architecture and Training Integration

We build FlexAM upon the Wan2.2Fun 5B Control model [1], a Transformer-based latent video diffusion

model. We adapt its conditioning mechanism to integrate our decoupled appearance and motion signals. The appearance condition  $\mathbf{V}_{\text{masked}}$  is processed by the VAE encoder to produce an appearance latent. To integrate the motion video, its components are first encoded by the VAE encoder. These latent representations are then fused and compressed by a CNN-based Adapter to generate the final motion control signal  $\mathbf{C}$ . To make the model aware of the control signal's sparsity, we introduce a scalar  $\mathbf{d}$  representing the point density, which is concatenated with the noise timestep embedding. We train our model for 12,000 steps using the AdamW optimizer on 16 H800 GPUs with a batch size of 16 and a learning rate of  $2 \times 10^{-5}$ .

### 3.4. Controllable Video Generation and Editing

In this section, we elaborate on how FlexAM achieves controllable video generation and video editing.

#### 3.4.1. Appearance Editing.

FlexAM innovatively decouples the appearance and motion of a video, enabling us to edit any part of the input video while preserving its dynamics, accomplishing tasks such as style transfer, character replacement, and virtual cinematography. First, we detect 3D points and their trajectories from the video, generating a motion video to represent the video's dynamics. Next, we create the video condition by prepending a repainted first frame to the subsequent frames of the masked video, where editable regions are filled with gray. Finally, FlexAM transfers the target appearance to the masked, to-be-edited regions according to the video dynamics preserved in the motion video, generating the target video.

#### 3.4.2. Camera Control.

FlexAM significantly enhances spatial awareness by introducing the frequency positional encoding  $\mathbf{f}_{\text{freq}} \in \mathbb{R}^{H \times W \times 12}$  and the depth-aware encoding  $\mathbf{f}_{\text{depth}} \in \mathbb{R}^{H \times W \times 3}$ , enabling precise camera control.

For the image-to-video generation task with a specific camera trajectory, we first estimate the depth map of the input image, which is then encoded using  $\mathbf{A}_i(t)$ . These points are then projected onto the given camera trajectory to construct a motion video, allowing FlexAM to control the camera motion precisely.

For the video-to-video camera control task, we first detect 3D points and trajectories and estimate the camera parameters and trajectory of the input video. Then we combined them to build a 4D dynamic point cloud. Subsequently, these points are projected onto the new camera trajectory to construct a new motion video for FlexAM to achieve high-precision camera re-cinematography.

#### 3.4.3. Spatial Object Editing.

FlexAM introducing the frequency positional encoding for precise control, and the depth-aware encoding attribute to avoid depth ambiguity during control. Given an image, we first estimate its depth map and segment the target object. We can then manipulate the point cloud of this object to construct a motion video for object manipulation video generation.

## 4. Experiment

We conduct experiments across three tasks — appearance editing, camera control, and spatial object editing — to demonstrate the versatility of FlexAM in video editing and controlling video generation.



Figure 3. Qualitative comparison on motion transfer between our method, DaS, Wan2.2 Fun, and VACE. We compare the results of different methods in transferring the human motion from the Source to a new appearance. Compared to the baseline, our method accurately transfers the motion.

### 4.1. Appearance Editing

We primarily compared FlexAM and the baseline on two subtasks: motion transfer and partial editing. In all appearance editing tasks, we used Qwen Image Edit [34] to generate the reference images.

#### 4.1.1. Motion Transfer

**Baseline.** We compare FlexAM with several famous motion transfer methods, DaS [10], VACE [15] and Wan2.2Fun (5B) Control [1]. We condition VACE (14B) and Wan2.2-Fun (5B) Control with depth maps, and use style-transferred images from Qwen Image Edit [34] as reference images.

**Metrics.** We use the CLIP [25] to evaluate the alignment between the generated videos and the text prompts and video coherence. Specifically, we extract multiple frames from the video and compare them with the corresponding text prompts by calculating the CLIP score [13] for each frame. This score reflects the alignment between image content and textual descriptions. For temporal consistency, we extract normalized CLIP features from adjacent video frames and compute the cosine similarity between the adjacent features.

**Results.** As shown in Table 1, our method demonstrates outstanding performance in both text alignment and frame consistency. Furthermore, Figure 3 presents the qualitative comparison of our method, DaS, VACE and Wan2.2Fun 5B Control. In Figure 3, VACE repainted the reference image during motion transfer, causing discrepancies in character ID from the original input. Wan2.2Fun 5B Control over-aligned with the depth map, resulting in distorted facial features. DaS failed to reconstruct the character’s pose. In contrast, FlexAM accurately transfers the video motion with strong temporal coherence.

	Tex-Ali $\uparrow$	Tem-Con $\uparrow$
DaS [10]	32.14	0.968
Wan2.2 Fun control [1]	32.39	0.971
VACE [15]	32.38	0.970
<b>FlexAM (Ours)</b>	<b>32.55</b>	<b>0.976</b>

Table 1. Performance Score Comparison of Different Models for Motion Transfer

#### 4.1.2. Partial Editing

**Baseline.** We compare FlexAM with VACE and Wan2.2Fun 5B Control on both foreground and background editing. Specifically, we used SAM2 [26] to mask the foreground or background of the input videos and expected these methods to accurately transfer the content from the corresponding masked areas in the reference images to the input videos, seamlessly integrate it with the motion in the masked regions of the input videos, and faithfully restore the unmasked parts of the original videos.

**Results.** As shown in Figure 4(a), for foreground editing, both methods generally follow the reference rhythm to synthesize the target foreground, but VACE frequently redraws the first-frame appearance and exhibits minor drifts at limb boundaries and contact regions; FlexAM better adheres to the reference rhythm while preserving identity and local de-

tails throughout the sequence. For background editing, as shown in Figure 4(b), while VACE maintains foreground object consistency with the input video, it fails to preserve background motion. In contrast, FlexAM successfully integrates the background motion from the input video with the background appearance of the reference image while preserving foreground consistency.

#### 4.2. Camera Control

**Baseline.** To validate the capability of FlexAM, we select three representative camera control models as baselines, namely DaS [10], Wan2.2 Fun Control Camera [1], and Re-CamMaster [2]. All methods receive the same camera trajectories as input.

**Metrics.** To measure the accuracy of the camera trajectories of generated videos, we evaluate the consistency between the estimated camera poses from the generated videos and the input ground-truth camera poses using rotation errors and translation errors. Specifically, for each frame of a generated video, we reconstruct its relative pose given the first frame using Pi3 [32]. Then, we get the normalized quaternion and translation vectors for the rotation and translation. Finally, we calculate the cosine similarity between the estimated camera poses with the given camera poses.

$$\text{RotErr} = \arccos\left(\frac{1}{T-1} \sum_{i=2}^T \langle q^i_{\text{gen}}, q^i_{\text{gt}} \rangle\right), \quad (6)$$

$$\text{TransErr} = \arccos\left(\frac{1}{T-1} \sum_{i=2}^T \langle t^i_{\text{gen}}, t^i_{\text{gt}} \rangle\right) \quad (7)$$

**Results.** We evaluate camera control performance on 100 random trajectories from RealEstate10K [39]. As shown in Table 2, FlexAM achieves the best performance in Rotation Error, significantly outperforming all baselines. Regarding Translation Error, while Wan2.2 [1] achieves a lower error rate, it is worth noting that Wan2.2 is a task-specific model explicitly trained with ground-truth camera poses as inputs. In contrast, FlexAM is a general-purpose framework that encodes camera motion implicitly via 3D point cloud projections, without specialized pose-conditioned modules. Despite lacking explicit pose supervision, our method delivers highly competitive translation accuracy while offering superior rotational stability, demonstrating the robustness of our unified representation. We further evaluated FlexAM against ReCamMaster and DaS on camera-controlled video re-rendering tasks using randomly selected internet videos. As shown in Figure 5, ReCamMaster exhibits rendering artifacts and trajectory deviation, while DaS fails to align with the target pose. In contrast, our method generates artifact-free results and precisely follows the target camera pose, demonstrating superior performance.



Figure 4. Qualitative comparison on foreground and background editing. We transfer the motion from the source videos while replacing the foreground/ background appearance using the reference prompt/image. (a) Replace bear with Godzilla; Compared to VACE, our method better follows the reference poses and preserves identity and color details. (b) Airplane wing over mountains at sunset; While VACE maintains foreground consistency but loses background motion, our method integrates the input video’s background motion with the new appearance, preserving coherent dynamics.



Figure 5. Qualitative comparison on camera control. We re-render the source video with the pan up-right target camera trajectory. ReCamMaster shows artifacts and deviates from the path; DaS fails to track the target pose. Our method closely matches the target trajectory while preserving appearance and temporal stability.

### 4.3. Spatial Object Editing

For spatial object editing, we adopt the SAM2 [26] and MoGe citemoge to get the object points. We compare FlexAM with DaS and GeoDiffuser [27] in two kinds of

	RotErr ↓	TransErr ↓
Da [10]	6.099	25.69
ReCamMaster [2]	1.935	36.24
Wan2.2 Fun Control Camera [1]	1.839	<b>17.49</b>
<b>FlexAM (Ours)</b>	<b>1.097</b>	23.70

Table 2. Quantitative results on camera control

tasks: translation and rotation. Since GeoDiffuser is an image-based manipulation method, we compare its results with the final video frame generated by FlexAM and DaS, and use the CLIP [25] to evaluate the alignment between the generated videos and the text prompts, as well as the video coherence.

	CLIP Scores ↑
GeoDiffuser [27]	0.9110
DaS [10]	0.9437
<b>FlexAM (Ours)</b>	<b>0.9536</b>

Table 3. Quantitative results for object manipulation.

**Results.** Table 3 demonstrates that FlexAM achieves accurate object manipulation to produce photorealistic videos with strong multiview consistency.

#### 4.4. Ablation Study

We conducted an ablation study of our improvements in motion video. Specifically, using DaS as the baseline, we performed a detailed analysis of the effectiveness of the improvements made by FlexAM’s motion video on DaS’s 3D Tracking Video – Control flexibility, Precise positional encoding, and Depth-aware encoding.

**Control Flexibility.** We evaluate robustness to sparsity via a video reconstruction task, where models are required with recovering original videos using only the first frame and extracted sparse motion signals. This enables quantitative assessment against the original video. As presented in Table 4, FlexAM significantly outperforms the baseline DaS [10] in reconstruction fidelity. The qualitative results in Figure 6 further illustrate this; our method maintains accurate motion control even with sparse conditions, demonstrating FlexAM’s capability to support control signals of different densities, thereby balancing flexibility and precision.

	PSNR $\uparrow$	SSIM $\uparrow$	FVD $\downarrow$
DaS [10]	18.2428	0.6458	625.3503
<b>FlexAM (Ours)</b>	<b>19.4958</b>	<b>0.6813</b>	<b>485.6534</b>

Table 4. Quantitative results for sparse control

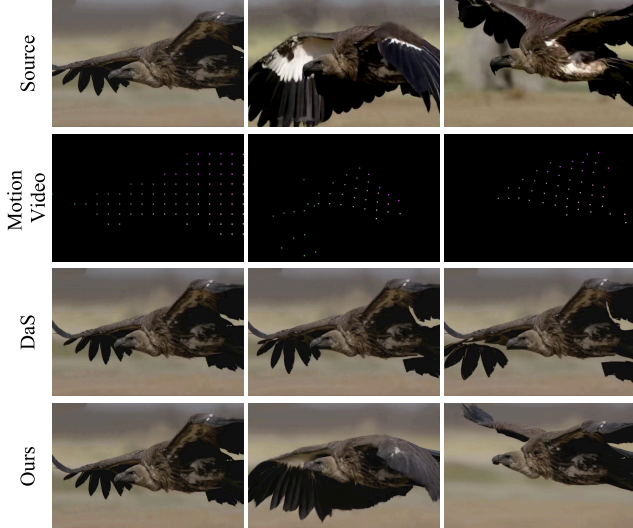


Figure 6. Qualitative comparison of control flexibility under sparse motion signals. We condition each method on low-density motion video in a bird flight case. Despite the sparse control, FlexAM maintains accurate motion while preserving the source appearance, consistent with our density-aware training that exposes the model to widely varying control densities. The baseline DaS, trained at a fixed density, degrades under sparsity—showing motion drift and shape inconsistencies.

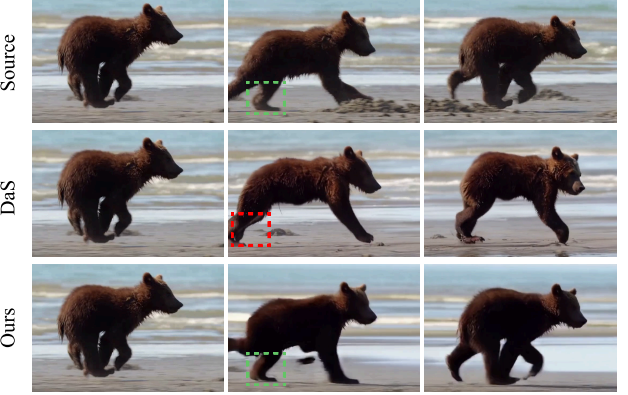


Figure 7. Qualitative comparison of precise positional encoding. FlexAM adds multi-frequency encodings to keep nearby points separable and motions consistent. The areas marked with color boxes demonstrate FlexAM’s better ability in reconstructing dynamic details compared to the baseline.



Figure 8. Qualitative comparison of depth-aware encoding. In object manipulation with little parallax (drawer opening), tracking-only DaS misinterprets the motion and yields physically implausible results; adding time-varying depth to the control signal lets our method recover the correct 3D trajectory and consistent geometry.

**Precise Positional Encoding.** As shown in Figure 7, baseline suffer from motion aliasing when screen-space trajectories overlap. This ambiguity causes the model to confuse or merge adjacent points, such as the bear’s left and right feet. Our use of a multi-frequency positional encoding, resolves this, enabling the model to preserve limb identity throughout the gait cycle. This yields temporally consistent contacts and plausible kinematics, in clear contrast to the baseline, which often swaps the feet.

**Depth-aware Encoding.** Figure 8 illustrates the impact of lacking video depth as a conditioning factor. Specifically, encoding 3D point clouds solely based on 2D screen-space coordinates fails to fully capture their spatial motion, as multiple distinct spatial movements can project to identical results in screen space. Consequently, as shown in Figure 8, relying exclusively on 2D screen-space coordinates for positional encoding in control signals introduces ambiguity. The baseline method, lacking depth conditioning, fails to accurately infer the object’s motion trajectory, producing results that violate real-world physics. In contrast, FlexAM correctly generates videos consistent with real-world physics.

## 5. Conclusions

**Conclusions.** We introduce FlexAM, a unified framework for controllable video generation that encodes scene dynamics as a dynamic 3D point cloud augmented with multi-frequency positional encodings, depth-aware encoding and flexible control. This control representation cleanly disentangles appearance from motion, enabling a single model to handle I2V/V2V editing, camera trajectory control, and object manipulation. Extensive experiments show consistent improvements over strong baselines, indicating that FlexAM achieves high precision without sacrificing generalization.

**Limitations.** FlexAM it still suffers from several limitations. First, inaccuracies in the tracking can diminish the precision of the resulting control, potentially affecting the fine-grained quality of the generated motion. Second, due to computational constraints, our model was trained on a dataset of a specific scale. Training on larger, web-scale video data could further enhance its robustness and ability to model more complex, long-range dynamics.

## References

[1] aigc apps. Videox-fun: A comprehensive video processing and ai-powered editing toolkit. <https://github.com/aigc-apps/VideoX-Fun>, 2024. Accessed: [Insert access date here]. 4, 6, 7

[2] Jianhong Bai, Menghan Xia, Xiao Fu, Xintao Wang, Lianrui Mu, Jinwen Cao, Zuozhu Liu, Haoji Hu, Xiang Bai, Pengfei Wan, and Di Zhang. Recammaster: Camera-controlled generative rendering from a single video, 2025. 2, 3, 6, 7

[3] Chenjie Cao, Jingkai Zhou, Shikai Li, Jingyun Liang, Chao-hui Yu, Fan Wang, Xiangyang Xue, and Yanwei Fu. Uni3c: Unifying precisely 3d-enhanced camera and human motion controls for video generation, 2025. 2, 3

[4] Liyang Chen, Tianxiang Ma, Jiawei Liu, Bingchuan Li, Zhuowei Chen, Lijie Liu, Xu He, Gen Li, Qian He, and Zhiyong Wu. Humo: Human-centric video generation via collaborative multi-modal conditioning, 2025. 2, 3

[5] Gang Cheng and Xin Gao et al. Wan-animate: Unified character animation and replacement with holistic replication, 2025. 2, 3

[6] Yufan Deng, Yuanyang Yin, Xun Guo, Yizhi Wang, Jacob Zhiyuan Fang, Shenghai Yuan, Yiding Yang, Angtian Wang, Bo Liu, Haibin Huang, and Chongyang Ma. Magref: Masked guidance for any-reference video generation with subject disentanglement, 2025. 2

[7] Ruoyu Feng, Wenming Weng, Yanhui Wang, Yuhui Yuan, Jianmin Bao, Chong Luo, Zhibo Chen, and Baining Guo. Ccredit: Creative and controllable video editing via diffusion models, 2024. 2

[8] Xin Gao and Li Hu et al. Wan-s2v: Audio-driven cinematic video generation, 2025. 2, 3

[9] Daniel Geng, Charles Herrmann, Junhwa Hur, Forrester Cole, Serena Zhang, Tobias Pfaff, Tatiana Lopez-Guevara, Carl Doersch, Yusuf Aytar, Michael Rubinstein, Chen Sun, Oliver Wang, Andrew Owens, and Deqing Sun. Motion prompting: Controlling video generation with motion trajectories, 2025. 2, 3

[10] Zekai Gu, Rui Yan, Jiahao Lu, Peng Li, Zhiyang Dou, Chenyang Si, Zhen Dong, Qifeng Liu, Cheng Lin, Ziwei Liu, Wenping Wang, and Yuan Liu. Diffusion as shader: 3d-aware video diffusion for versatile video generation control. In *Proceedings of the Special Interest Group on Computer Graphics and Interactive Techniques Conference Conference Papers*, New York, NY, USA, 2025. Association for Computing Machinery. 2, 3, 4, 6, 7, 8

[11] Yoav HaCohen and Nisan Chiprut et al. Ltx-video: Realtime video latent diffusion, 2024. 2

[12] Hao He, Yinghao Xu, Yuwei Guo, Gordon Wetzstein, Bo Dai, Hongsheng Li, and Ceyuan Yang. Cameractrl: Enabling camera control for text-to-video generation, 2025. 2, 3

[13] Jack Hessel, Ari Holtzman, Maxwell Forbes, Ronan Le Bras, and Yejin Choi. Clipscore: A reference-free evaluation metric for image captioning, 2022. 6

[14] Teng Hu, Zhentao Yu, Zhengguang Zhou, Sen Liang, Yuan Zhou, Qin Lin, and Qinglin Lu. Hunyuancustom: A multimodal-driven architecture for customized video generation, 2025. 2

[15] Zeyinzi Jiang, Zhen Han, Chaojie Mao, Jingfeng Zhang, Yulin Pan, and Yu Liu. Vace: All-in-one video creation and editing, 2025. 2, 3, 6

[16] Xuan Ju, Tianyu Wang, Yuqian Zhou, He Zhang, Qing Liu, Nanxuan Zhao, Zhifei Zhang, Yijun Li, Yuanhao Cai, Shaoteng Liu, Daniil Pakhomov, Zhe Lin, Soo Ye Kim, and Qiang Xu. Editverse: Unifying image and video editing and generation with in-context learning, 2025. 2

[17] Jun Hao Liew, Hanshu Yan, Jianfeng Zhang, Zhongcong Xu, and Jiashi Feng. Magicedit: High-fidelity and temporally coherent video editing, 2023. 2, 3

[18] Bin Lin, Yunyang Ge, Xinhua Cheng, Zongjian Li, Bin Zhu, Shaodong Wang, Xianyi He, and Yang Ye et al. Open-sora plan: Open-source large video generation model, 2024. 2

[19] Pengyang Ling, Jiazi Bu, Pan Zhang, Xiaoyi Dong, Yuhang Zang, Tong Wu, Huaiyan Chen, Jiaqi Wang, and Yi Jin. Motionclone: Training-free motion cloning for controllable video generation, 2024. 2

[20] Lijie Liu, Tianxiang Ma, Bingchuan Li, Zhuowei Chen, Jiawei Liu, Gen Li, Siyu Zhou, Qian He, and Xinglong Wu. Phantom: Subject-consistent video generation via cross-modal alignment, 2025. 2

[21] Shaoteng Liu, Yuechen Zhang, Wenbo Li, Zhe Lin, and Jiaya Jia. Video-p2p: Video editing with cross-attention control, 2023. 2, 3

[22] Yue Ma, Yulong Liu, Qiyuan Zhu, Ayden Yang, Kunyu Feng, Xinhua Zhang, Zhifeng Li, Sirui Han, Chenyang Qi, and Qifeng Chen. Follow-your-motion: Video motion transfer via efficient spatial-temporal decoupled finetuning, 2025. 2, 3

[23] Rang Meng, Xingyu Zhang, Yuming Li, and Chenguang Ma. Echomimicv2: Towards striking, simplified, and semi-body human animation, 2025. 3

[24] Liao Qu, Huichao Zhang, Yiheng Liu, Xu Wang, Yi Jiang, Yiming Gao, Hu Ye, Daniel K. Du, Zehuan Yuan, and Xinglong Wu. Tokenflow: Unified image tokenizer for multi-modal understanding and generation, 2025. 2, 3

[25] Alec Radford, Jong Wook Kim, Chris Hallacy, Aditya Ramesh, Gabriel Goh, Sandhini Agarwal, Girish Sastry, Amanda Askell, Pamela Mishkin, Jack Clark, Gretchen Krueger, and Ilya Sutskever. Learning transferable visual models from natural language supervision, 2021. 6, 7

[26] Nikhila Ravi, Valentin Gabeur, Yuan-Ting Hu, Ronghang Hu, Chaitanya Ryali, Tengyu Ma, Haitham Khedr, Roman Rädle, Chloe Rolland, Laura Gustafson, Eric Mintun, Junting Pan, Kalyan Vasudev Alwala, Nicolas Carion, Chao-Yuan Wu, Ross Girshick, Piotr Dollár, and Christoph Feichtenhofer. Sam 2: Segment anything in images and videos, 2024. 6, 7

[27] Rahul Sajnani, Jeroen Vanbaar, Jie Min, Kapil Katyal, and Srinath Sridhar. Geodiffuser: Geometry-based image editing with diffusion models, 2025. 4, 7

[28] Meituan LongCat Team, Bayan, Bei Li, Bingye Lei, and Bo Wang et al. Longcat-flash technical report, 2025. 2

[29] Team Wan, Ang Wang, Baole Ai, Bin Wen, and Chaojie Mao et al. Wan: Open and advanced large-scale video generative models, 2025. 2

[30] Mengchao Wang, Qiang Wang, Fan Jiang, Yaqi Fan, Yunpeng Zhang, Yonggang Qi, Kun Zhao, and Mu Xu. Fantasytalking: Realistic talking portrait generation via coherent motion synthesis, 2025. 2, 3

[31] Qinghe Wang, Yawen Luo, Xiaoyu Shi, Xu Jia, Huchuan Lu, Tianfan Xue, Xintao Wang, Pengfei Wan, Di Zhang, and Kun Gai. Cinemaster: A 3d-aware and controllable framework for cinematic text-to-video generation, 2025. 2, 3

[32] Yifan Wang, Jianjun Zhou, Haoyi Zhu, Wenzheng Chang, Yang Zhou, Zizun Li, Junyi Chen, Jiangmiao Pang, Chunhua Shen, and Tong He.  $\pi^3$ : Permutation-equivariant visual geometry learning, 2025. 6

[33] Zhouxia Wang, Ziyang Yuan, Xintao Wang, Tianshui Chen, Menghan Xia, Ping Luo, and Ying Shan. Motionctrl: A unified and flexible motion controller for video generation, 2024. 2, 3

[34] Chenfei Wu, Jiahao Li, Jingren Zhou, Junyang Lin, Kaiyuan Gao, Kun Yan, Shengming Yin, Shuai Bai, Xiao Xu, Yilei Chen, Yuxiang Chen, Zecheng Tang, Zekai Zhang, Zhengyi Wang, An Yang, Bowen Yu, Chen Cheng, Dayiheng Liu, Deqing Li, Hang Zhang, Hao Meng, Hu Wei, Jingyuan Ni, Kai Chen, Kuan Cao, Liang Peng, Lin Qu, Minggang Wu, Peng Wang, Shuteng Yu, Tingkun Wen, Wensen Feng, Xiaoxiao Xu, Yi Wang, Yichang Zhang, Yongqiang Zhu, Yujia Wu, Yuxuan Cai, and Zenan Liu. Qwen-image technical report, 2025. 5, 6

[35] Weijia Wu, Zhuang Li, Yuchao Gu, Rui Zhao, Yefei He, David Junhao Zhang, Mike Zheng Shou, Yan Li, Tingting Gao, and Di Zhang. Draganything: Motion control for anything using entity representation, 2024. 2, 3

[36] Shaoshu Yang, Zhe Kong, Feng Gao, Meng Cheng, Xiangyu Liu, Yong Zhang, Zhuoliang Kang, Wenhan Luo, Xunliang Cai, Ran He, and Xiaoming Wei. Infinitetalk: Audio-driven video generation for sparse-frame video dubbing, 2025. 2, 3

[37] Zhuoyi Yang, Jiayan Teng, Wendi Zheng, Ming Ding, Shiyu Huang, Jiazheng Xu, Yuanming Yang, Wenyi Hong, Xiaohan Zhang, Guanyu Feng, Da Yin, Yuxuan Zhang, Weihang Wang, Yean Cheng, Bin Xu, Xiaotao Gu, Yuxiao Dong, and Jie Tang. Cogvideox: Text-to-video diffusion models with an expert transformer, 2025. 2

[38] Zhenghao Zhang, Junchao Liao, Menghao Li, Zuozhuo Dai, Bingxue Qiu, Siyu Zhu, Long Qin, and Weizhi Wang. Tora: Trajectory-oriented diffusion transformer for video generation, 2025. 2, 3

[39] Tinghui Zhou, Richard Tucker, John Flynn, Graham Fyffe, and Noah Snavely. Stereo magnification: Learning view synthesis using multiplane images. In *SIGGRAPH*, 2018. 6

# FlexAM: Flexible Appearance-Motion Decomposition for Versatile Video Generation Control

## Supplementary Material

### 6. Visualization of Motion Video

#### Algorithm 1 Visualization of Motion Video $\mathbf{f}_{\text{identity}}, \mathbf{f}_{\text{freq}}, \mathbf{f}_{\text{depth}}$

```

1: function VISUALIZE MOTION VIDEO( $\mathbf{P}_{T \times N \times 3}$ ,  $\mathbf{M}_{T \times N}$ , mode)
2:   Color Encoding (per point):
3:   for  $i = 1, \dots, N$  do
4:      $(x'_i(0), y'_i(0), z'_i(0)) = (x_i(0), y_i(0), \frac{1}{z_i(0)+\epsilon})_{\text{norm} \rightarrow [0, 1]^3}$ 
5:     if mode = IDENTITY then
6:        $c_i \leftarrow (x'_i(0), y'_i(0), z'_i(0))$   $\triangleright \mathbf{f}_{\text{identity}} \in \mathbb{R}^3$ 
7:     else if mode = FREQ then
8:        $c_i \leftarrow (\gamma(x'_i(0)), \gamma(y'_i(0)), \gamma(z'_i(0)))_{\text{norm} \rightarrow [0, 1]^{12}}$   $\triangleright \mathbf{f}_{\text{freq}} \in \mathbb{R}^{12}$ 
9:   Frame-wise Rendering:
10:  for each frame  $t \in [1, T]$  do
11:    if mode = DEPTH then  $\triangleright \mathbf{f}_{\text{depth}} \in \mathbb{R}^3$ 
12:      for  $i = 1, \dots, N$  do
13:         $c_i(t) \leftarrow \mathcal{S}((z_i(t))_{\text{norm} \rightarrow [0, 1]})$   $\triangleright \mathbf{f}_{\text{depth}} \in \mathbb{R}^3$ 
14:         $V_t \leftarrow P_t \odot M_t$   $\triangleright$  mask out invisible points
15:        pixels  $\leftarrow \text{Project2D}(V_t^{x, y})$   $\triangleright 3D \rightarrow 2D$  pixel coordinates
16:        if mode  $\in \{\text{IDENTITY}, \text{FREQ}\}$  then
17:           $\{\text{pix}^\downarrow, c^\downarrow\} \leftarrow \text{SortByDepth}(V_t^z, \{c_i\}_{i=1}^N)$ 
18:        else  $\triangleright$  mode = DEPTH
19:           $\{\text{pix}^\downarrow, c^\downarrow\} \leftarrow \text{SortByDepth}(V_t^z, \{c_i(t)\}_{i=1}^N)$ 
20:        DRAWCOLORBLOCKS( $\text{pix}^\downarrow, c^\downarrow$ )  $\triangleright$  paint  $k \times k$  color patches at each
pixel
21:  return ComposeVideo( $\{I_t\}$ )  $\triangleright$  encode all rendered frames into a video

```

To visualize the different 3D encodings, we use a unified rendering procedure as summarized in Alg. 1. The function takes as input a trajectory tensor  $\mathbf{P}_{T \times N \times 3}$  and a binary visibility mask  $\mathbf{M}_{T \times N}$ , together representing a set of 3D point trajectories  $\mathbf{p}_i(t) \in \mathbb{R}^3$ . Each point  $\mathbf{p}_i(t) = (x_i(t), y_i(t), z_i(t))$  corresponds to a specific spatial region. In the case of the identity encoding  $\mathbf{f}_{\text{identity}}$ , we first perform a *color encoding* step on the initial 3D coordinates. For every point  $i$ , we normalize its initial position and construct  $(x'_i(0), y'_i(0), z'_i(0))$  from  $(x_i(0), y_i(0), 1/(z_i(0) + \epsilon))$ , where the inverse-depth term and a small constant  $\epsilon$  avoid numerical instabilities. These normalized components are then directly interpreted as RGB values, yielding a static color code  $c_i \in [0, 1]^3$  that uniquely identifies each point and remains fixed over time.

Given these per-point colors, frame generation proceeds identically for all timesteps. At each time  $t$ , we first mask out invisible points to obtain  $\mathbf{V}_t = \mathbf{P}_t \odot \mathbf{M}_t$ , and project the visible 3D coordinates to 2D screen space via  $\text{Project2D}(\cdot)$ , which converts normalized  $(x, y)$  values into integer pixel locations. To correctly handle occlusions, we apply  $\text{SortByDepth}(\cdot)$  to order points by their depth (using  $z$ ) before rendering, and pass the resulting pixel co-

ordinates and colors to the  $\text{DrawColorBlocks}(\cdot)$  routine. This subroutine paints fixed-size  $k \times k$  color patches (with  $k = \text{pointsize}$ ) at each projected location, yielding a rendered frame  $I_t$ . Finally, all frames are encoded into a video through  $\text{ComposeVideo}(\cdot)$ , producing a dense visualization of the underlying 3D motion.

The multi-frequency visualization for  $\mathbf{f}_{\text{freq}}$  reuses this rendering pipeline and differs only in the color encoding step. Instead of directly mapping the normalized coordinates  $(x'_i(0), y'_i(0), z'_i(0))$  to RGB, we first apply a multi-frequency cosine embedding  $\gamma(\cdot)$  to each coordinate and concatenate the resulting features. The 12-dimensional vector  $[\gamma(x'_i(0)), \gamma(y'_i(0)), \gamma(z'_i(0))]$  is then normalized back to  $[0, 1]^3$  to obtain a color  $c_i$  that encodes richer high-frequency spatial information while remaining visually interpretable. As in the identity case, these colors are static over time; only the 3D positions change across frames.

In contrast, the depth-aware visualization for  $\mathbf{f}_{\text{depth}}$  keeps the projection, depth sorting, and rendering stages unchanged, but makes the color field explicitly time-dependent. Rather than assigning a fixed color from the initial frame, we compute a per-frame color  $c_i(t)$  based solely on the current normalized depth  $z''_i(t)$ . This scalar depth is mapped through a colormap  $\mathcal{S}(\cdot)$  (e.g., Spectral) to produce an RGB value  $c_i(t) \in [0, 1]^3$ , so that near and far points are visually separated and their depth evolution over time becomes directly observable. The subsequent steps—projection to 2D, depth-based ordering, and drawing colored patches—are identical to the identity and multi-frequency variants; the only change is whether the color encodes a static 3D identity (identity / multi-frequency) or a dynamic, depth-aware signal (depth).

### 6.1. Generate Motion Video in Appearance Editing

In the appearance editing setting, we take the source video as input and, when performing foreground/background editing, apply the SAM2 model to detect and segment the object to be edited, obtaining a binary mask (for motion transfer, this segmentation step is skipped). We then use DELTA as a 3D tracker to extract the source video's 3D tracking points  $\mathbf{P}_{T \times N \times 3}$  and a binary visibility mask  $\mathbf{M}_{T \times N}$ , where the density of tracking points is controlled by a down-sampling factor (with a maximum density of  $512 \times 384$  points when the factor is set to 1). The binary mask from SAM2 is further used to refine  $\mathbf{M}_{T \times N}$  by keeping only the tracking points that belong to the object to be edited, while in motion transfer tasks all tracking points are retained. We employ

Qwen Edit to redraw the first frame of the source video, either fully or partially, corresponding to motion transfer or foreground/background editing, respectively. In the subsequent frames, unedited regions preserve their original pixel values, whereas regions to be regenerated are overwritten with a gray value of 127. In typical foreground editing scenarios, the region covered by this gray value is slightly larger than the region indicated by the binary mask, so as to handle possible shape mismatches between the redrawn object and the original one.

## 6.2. Generate Motion Video in Camera Control

For the image + camera trajectory (I2V) setting, we first use MoGe2 to estimate a depth map from the input image and convert this depth map into a 3D point cloud, yielding initial 3D positions  $\mathbf{p}_i(0)$ . These 3D points are then reprojected along a prescribed camera trajectory, producing their pixel coordinates  $(u_i(t), v_i(t))$  and depth values under each virtual viewpoint. Collecting these per-frame 3D positions results in the trajectory tensor  $\mathbf{P}_{T \times N \times 3}$  used as the camera-controlled motion signal.

For the video + camera trajectory (V2V) setting, we first apply DELTA as a 3D tracker to obtain the source video’s 3D tracking points  $\mathbf{P}_{T \times N \times 3}$ . In parallel, we use VGGT to estimate the camera intrinsics and extrinsics of the input video, thereby recovering its camera parameters and trajectory. Combining the tracked image-space coordinates with the estimated intrinsics and extrinsics yields a 4D dynamic point cloud, where each point has a 3D position in the world coordinate system at every frame. This dynamic point cloud is then reprojected onto a new, user-specified camera trajectory to obtain updated pixel coordinates and depths  $(u_i(t), v_i(t), z_i(t))$ , forming a camera-controlled version of the original motion.

## 6.3. Generate Motion Video in Spatial Object Editing

In the spatial object editing setting, we start from a single input image and use MoGe2 to estimate a depth map, which is then converted into a 3D point cloud  $\mathbf{p}_i(0)$ . SAM2 is applied to segment the target object, and the resulting object mask is used to select only the 3D points belonging to that object. Given a user-specified object motion trajectory, we manipulate the corresponding object point cloud over time—translating, rotating, or otherwise editing its 3D positions—while keeping the background points fixed. This procedure yields an object-centric dynamic point cloud evolving over time, which we denote as  $\mathbf{P}_{T \times N \times 3}$ .

## 7. Details of Training Datasets

Our training set comprises 72,617 videos, including 22,931 randomly sampled from OpenVid-1M and the remainder

randomly sampled from Koala-36M. The dataset is dominated by three resolutions—1280×720 (58.8%), 576×320 (35.8%), and 768×480 (5.1%)—while all other resolutions (e.g., 1024×1024, 480×384, 720×1280) together constitute only a negligible proportion.

To construct the tracking videos, we render the 3D points estimated by DELTA onto the image plane. To obtain motion controls with varying spatial sparsity, we evenly split the ~72k training videos into six subsets and generate the motion video for each subset using a distinct down-sampling stride (5, 10, 15, 20, 25, 30), thereby covering different granularities of point density and control.

## 8. Run Time

In the inference stage, we employ the Discrete Flow Matching sampler with 50 steps, classifier-free guidance of magnitude 6.0, which costs about 71 seconds to generate 49 frames on a A800 GPU at a resolution of 512×768.

## 9. Additional Qualitative Results



Figure 9. Qualitative comparison on object manipulation. Top: translation; bottom: rotation. We edit the masked object while keeping the scene unchanged. FlexAM preserves identity and contact and handles self-occlusion, while GeoDiffuser struggles to maintain object identity and DaS incorrectly rotates non-target regions.

Figure 9 presents more results for the object manipulation task, where our method better preserves object identity and contact and avoids unintended motion in non-target regions compared to GeoDiffuser and DaS.